# Residual Stress Effects in Stress-Corrosion Cracking

*J. Toribio*

*(Submitted 15 August 1997; in revised form 26 September 1997)*

**This paper describes a wide variety of residual stress effects in stress-corrosion cracking (SCC) of metallic materials on the basis of previous research of the author on high-strength steel in the form of hot-rolled bars and cold-drawn wires for prestressed concrete. It is seen that internal residual stress fields in the material play a very important—if not decisive—role in the SCC behavior of any engineering material, especially residual stresses generated near the free surface or in the vicinity of a crack tip.**

**Keywords** hydrogen embrittlement, residual stresses, stress-corrosion cracking

## 1. Introduction

Residual stresses may be present in metallic materials, mainly near the surface, due to thermomechanical treatments associated with the manufacturing process (hot rolling, cold drawing, welding, etc.). Many times internal residual stress fields are an undesired, although unavoidable, consequence of the industrial production.

In addition, when a crack is present in the material, cyclic loading due to the engineering conditions or experimental fatigue precracking for stress-corrosion cracking (SCC) testing in laboratory generate cyclic residual stresses of a compressive nature in the vicinity of the crack tip which has been previously subjected to far-field cyclic tension. This is due to the plastic zone created by the load in the vicinity of the crack tip, surrounded by an elastic region which compresses the former to achieve compatibility of strains, thus creating compressive residual stresses that tend to close the crack tip over some distance.

In this report both the effects of manufacturing and cyclic residual stresses on SCC are reviewed, as well as the combination of the two items: residual stresses generated by cyclic loading but influenced by the manufacturing process. Because hydrogen is present in most SCC processes due to local electrochemical conditions and its effect is deleterious on the resistance properties of metallic materials, the analysis is mainly focused on hydrogen-assisted cracking (or hydrogen embrittlement) processes.

## 2. Manufacturing Residual Stresses

### *2.1 Residual Stress Effects of Manufacturing a Cold-Drawn Wire*

Internal residual stresses in the material play an important role, since they transform a uniform stress state into a nonuniform one. In the particular case of wire structural elements analyzed in this paper, cold drawing generates residual stress fields in the wires, with more pronounced gradients near the surface. In Fig. 1 a plot is given of the axial residual stress distributions measured in high-strength steel wires after different thermomechanical processes (Ref 1). The axial (zz) component (that parallel to the wire axis) of the stress tensor was measured at different depths from the wire surface (radial direction) by the electrolitic polishing method and x-ray diffraction, showing that they can be tensions or compressions.

The importance of residual stresses in affecting the posterior fatigue behavior of the material is now well known. The local stress state in the vicinity of the surface is relevant to nucleate short fatigue cracks near the surface, and it can even affect the growth of macroscopic (engineering) cracks. The superposition principle in linear elastic fracture mechanics demonstrates that the stress-intensity factor is affected by the previous residual stress fields in the material.

In addition, it is now well known that residual stress fields can accelerate or delay (depending on their tensile or compressive nature) the environmentally assisted degradation process, mainly in those situations associated with the presence of hydrogen. The reason is that they modify the stress state in the vicinity of the element surface and influence hydrogen entry and diffusion toward the fracture process zone. The hydrogen embrittlement susceptibility of high-strength cold-drawn wires is reported in the following section.

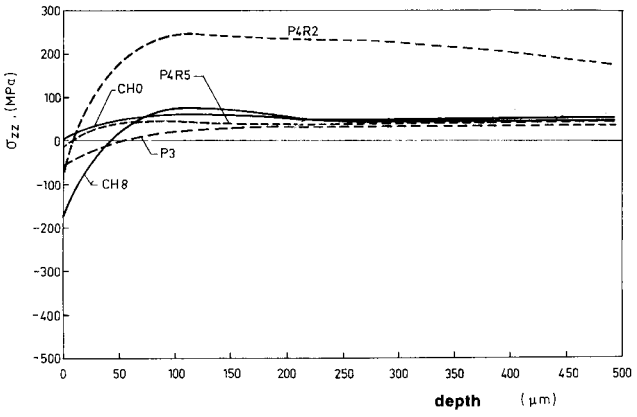


**Fig. 1** Axial residual stress distributions measured in high-strength steel wires after different thermomechanical processes, for a wire radius of 7 mm and a material yield strength of 1500 MPa. Source: Ref 1

**J. Toribio,** Department of Materials Science, University of La Coruña, ETSI Caminos, Campus de Elviña, 15192 La Coruña, Spain.

### 2.2 *Consequences in Hydrogen-Assisted Cracking of the Wires*

Reference 2 offers results of a wide experimental program on hydrogen-assisted cracking of prestressing steel wires, following the standard test in ammonium thiocyanate proposed by the International Prestressing Federation (FIP) to measure the susceptibility of prestressing steels to hydrogen embrittlement. Four commercial prestressing steel wires were tested according to the FIP tests in an aqueous environment promoting hydrogen-assisted cracking. All them were cold-drawn pearlitic steels, produced by patenting 12 mm diameter rods in a molten lead bath at 530 °C for about 10 s to produce fine pearlite, after which the rods were cold-drawn to achieve 7 mm diameter wires. Finally, the drawn wires were stress relieved at 425 °C for a few seconds and cooled in water or oil. Their chemical compositions are shown in Table 1 and their mechanical properties are summarized in Table 2. The microstructure of the four cold-drawn steels consisted of fine pearlite with an average pearlite interlamellar spacing of about 0.03 μm.

Specimens used for testing were smooth round wires with their surface in the as-delivered condition and loaded at constant load by means of levers, as described elsewhere (Ref 2). If no fracture occurred in a given time, the specimen was unloaded and the time recorded, in order to obtain a threshold stress value. This was never under 600 h. For each stress level, at least four tests were performed, and in many cases eight tests were carried out.

The results are shown in Fig. 2 for the four tested steels. For each level of externally applied stress $\sigma_{ap}$, the average time to rupture $t_R$ (or critical time) and the interval corresponding to the standard deviation are plotted. Two important observations can be made from these results. First, these tests present a high level of scattering in time to rupture, a variable that reflects the susceptibility of the metal to hydrogen embrittlement (or hydrogen-assisted cracking). Second, the scattering is non-uniform, but for high stress levels it is small and clearly increases when the applied stress is lower. The explanation should be sought in any variable able to modify the externally applied stress state. In this conceptual framework, surface residual stresses in the material may be the cause of these phenomena .

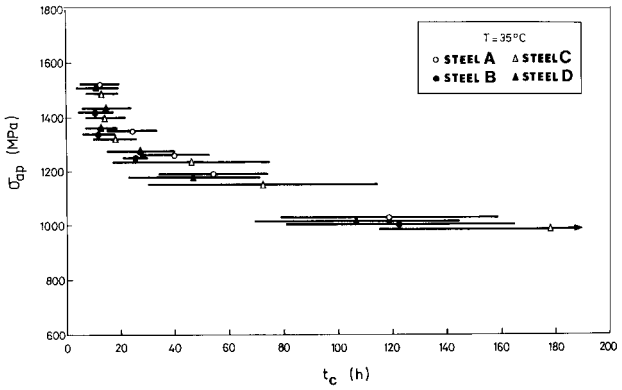


**Fig. 2** Experimental results of the International Prestressing Federation tests under a hydrogen environment, in the form of externally applied stress ($\sigma_{ap}$) vs. time to rupture $t_R$ (or critical time). The interval corresponding to the standard deviation is also plotted.

### 2.3 *Modeling of the Environmental Process: Life Prediction*

Reference 3 describes a diffusion-based computer model to predict the operational life of structural elements working in a hydrogen environment produced by the surrounding aggressive atmosphere. The model allows the introduction of computations of residual stress laws that influence the hydrogen concentration at the surface and the hydrogen diffusion toward the inner points, thus conditioning the life of the structural member in the harsh environment. Therefore the model predictions can be compared with the experimental results of the FIP tests in ammonium thiocyanate.

**Diffusion Equations.** The equations describing the hydrogen diffusion from the environment into the metal are based on three main hypotheses:

- *D1. Hypothesis of Absorption:* The absorption of adsorbed hydrogen at the metal surface is considered quasi-instantaneous.
- *D2. Hypothesis of Transport:* It is assumed that the main hydrogen transport mechanism is stress-assisted diffusion.
- *D3. Hypothesis of Cylindrical Symmetry:* The hydrogen entry and diffusion toward the inner points are assumed to possess cylindrical symmetry, i.e., every point of a circumference with its center at the cylinder axis is supposed to receive the same amount of hydrogen, the concentration depending only on the radial length (distance from the free surface).

From hypothesis D2, the equations for stress-assisted diffusion are modified Fick's laws to include terms dependent on the hydrostatic stress (Ref 3):

$$J = -D(\nabla c - \frac{V^*}{RT}\, c\nabla s) \qquad \text{(Eq 1)}$$

$$\frac{\partial c}{\partial t} = D(\Delta c - \frac{V^*}{RT}\nabla c \cdot \nabla s - \frac{V^*}{RT}\, c\Delta s) \qquad \text{(Eq 2)}$$

where $c$ is the hydrogen concentration, $J$ is the hydrogen flux, $t$ is the time, $s$ is the hydrostatic stress ($s$ = tr $\sigma$/3), $D$ is the hydrogen diffusion coefficient , $V^*$ is the molar partial volume of hydrogen, $R$ is the ideal gases constant, and $T$ is the absolute temperature. The term $\Delta$ indicates the Laplacian operator ($\Delta$ = div grad).

From hypothesis D1, the concentration of hydrogen at the inner sample surface ($c_0^*$) is quasi-instantaneously reached, which means that it is a direct function of the hydrostatic stress:

**Table 1 Chemical composition (wt%) os steels used in FIP tests**

| Steel | C | Mn | Si | P | S | N |
|---|---|---|---|---|---|---|
| A | 0.82 | 0.60 | 0.18 | 0.010 | 0.024 | 0.007 |
| B, C, D | 0.81 | 0.60 | 0.27 | 0.014 | 0.029 | 0.011 |

$$c_0^* = c_0 \exp\left(\frac{V^* s_\Gamma}{RT}\right) \quad \text{(Eq 3)}$$

This is a Boltzmann's distribution where $c_0$ is the equilibrium concentration for the metal-environment system when the former is free of stress, and $s_\Gamma$ is the hydrostatic stress at the boundary.

The stationary solution of the diffusion partial differential equation, Eq 2, is also a distribution of the Boltzmann type:

$$c_0(x) = c_0 \exp\left(\frac{V^* s(x)}{RT}\right) \quad \text{(Eq 4)}$$

where $x$ indicates any point of the domain.

Following hypothesis D3, the diffusion problem is that of a cylinder of radius $a$ and $c = c_0^*$ as the concentration at the inner boundary ($r = a$ and $x = 0$, $r$ and $z$ being cylindrical coordinates and $x$ the depth). Taking into account the cylindrical symmetry, the diffusion equation leads to:

$$\frac{\partial c}{\partial t} = D\left(\frac{\partial^2 c}{\partial r^2} + \frac{1}{r}\frac{\partial c}{\partial r}\right) - \frac{DV^*}{RT}\frac{\partial c}{\partial r}\frac{\partial s}{\partial r} - \frac{DV^*}{RT}c\left(\frac{\partial^2 s}{\partial r^2} + \frac{1}{r}\frac{\partial s}{\partial r}\right) \quad \text{(Eq 5)}$$

in the interval $0 \le r \le a$, with the initial condition:

$$c\,(r, 0) = 0 \quad \text{(Eq 6)}$$

and the boundary conditions:

$$\frac{\partial c}{\partial r}(0, t) = 0;\ t \ge 0 \quad \text{(Eq 7)}$$

$$c\,(a, t) = c_0^*;\ t \ge 0 \quad \text{(Eq 8)}$$

**Fracture Criterion.** The following hypotheses are adopted with regard to the fracture process in hydrogen:

- *F1. Hypothesis of Damage Localization:* The fracture phenomenon is spatially localized and the damage is assumed to be concentrated as a discrete part-through crack perpendicular to the bar axis, thus losing the cylindrical symmetry.
- *F2. Hypothesis of Initiation:* Fracture initiates when the hydrogen reaches a critical concentration $c_c$ over a distance $x_c$ (process zone, damaged area, or critical size for initiation); then it is assumed that a crack of depth $x_c$ is created (embrittled zone).
- *F3. Hypothesis of Propagation:* The propagation time, i.e., the time required to propagate the crack from the initial size $x_c$ up to a critical value for final fracture, is neglected. Then it is assumed that the initiation time coincides with the time to fracture or critical time $t_c$.

With hypothesis F1 the fracture phenomenon is modeled as a damage process spatially localized, whereas hypotheses F2 and F3 imply a time localization. This implies that initiation and fracture criteria are equivalent and that there is no subcritical crack growth.

**Life Prediction.** Residual stress distributions generated in the vicinity of the wire surface during the manufacturing process can be introduced into the model, thus influencing the hydrogen entry. Six laws were considered (Fig. 3a). Distribution 1 is that of a material free of residual stresses; laws 2, 3, 4, and 5 correspond to materials with positive and negative residual stresses associated with the manufacturing process. Plot 6 represents a material that has undergone a rolling process after manufacture, introducing strong compressive residual stresses.

Figure 3(b) shows model predictions compared with the experimental scattering band of Fig. 2 (shaded area). The agreement is excellent, because curve 1 exactly fits the central tendency, and curves 2, 3, 4, and 5 cover the experimental band. Compressive residual stresses extend the life of the wires, while tensile residual stresses decrease it. Very strong residual stresses (curve 6) extend the wire life even more. The importance of the externally applied stress in the scattering of the results (higher for lower stresses) is thus emphasized.

## 3. Cyclic Residual Stresses

### *3.1 Residual Stress Effects of Fatigue Precracking*

Experimental evaluation of SCC is usually achieved in the framework of fracture mechanics, by means of constant load testing, constant strain testing, or slow strain rate testing. For this purpose, the only consensus standard currently fully developed is ISO 7539 (Ref 4).

Although a variety of specimens (initially plain, notched, and precracked) can be used, ISO 7539-6 is devoted to precracked samples. These specimens present clear advantages because they are quite realistic—crack-like defects are very frequent in structural materials—and because the effect of the environment is localized in the vicinity of the crack tip, apart from the fact that fracture mechanics techniques are applicable.

**Table 2 Mechanical properties of steels used in FIP tests**

| Steel | 0.2% offset yield strength, MPa | Ultimate tensile strength (UTS), MPa | Elongation under UTS, % | Reduction, of area, % | $K_{Ic}$, MPa$\sqrt{m}$ |
|---|---|---|---|---|---|
| A | 1455 | 1700 | 6.0 | 30.0 | 98 |
| B | 1460 | 1681 | 5.5 | 29.5 | 98 |
| C | 1410 | 1653 | 5.6 | 27.2 | 98 |
| D | 1460 | 1682 | 5.5 | 27.0 | 98 |

Cyclic residual stresses, the compressive type, generated near the crack tip during the fatigue precracking procedure play an important role in SCC and produce an extremely high scatter in experimental results if they are not carefully controlled during the test. These effects have been considered in ISO 7539-6, which recommends that precracking should be completed below the expected SCC threshold $K_{ISCC}$ if possible.

### 3.2 Consequences in the Stress-Corrosion Cracking Threshold

The consequences of cyclic residual stresses in the initiation of SCC were analyzed in a previous work (Ref 5). It dealt with the influence of the maximum stress-intensity factor during fatigue precracking ($K_{max}$) on the SCC threshold $K_{ISCC}$ of a high-strength prestressing steel (in the form of hot-rolled bar), distinguishing between the two main corrosion phenomena associated with eutectoid steels in aqueous environments: localized anodic dissolution and hydrogen-assisted cracking.

The thresholds were measured by means of constant-strain tests, as described elsewhere (Ref 5). Figure 4 gives the SCC thresholds $K_{ISCC}$ for hydrogen-assisted cracking ($K_{IHAC}$) and localized anodic dissolution ($K_{ILAD}$) as a function of the maximum stress-intensity factor during the last stage of fatigue precracking ($K_{max}$). Therefore the threshold ($K_{ISCC}$) does not seem to have an intrinsic character, but rather depends on certain variables such as the maximum stress-intensity level during the last step of fatigue precracking, which strongly influences the threshold itself, as shown in Fig. 4. Values are divided by the critical stress intensity factor $K_{Ic}$ and the rough tendencies are the following:

$$(K_{IHAC}/K_{Ic}) = 0.12 + 0.92\,(K_{max}/K_{Ic}) \quad \text{(Eq 9)}$$

$$(K_{ILAD}/K_{Ic}) = 0.54 + 0.84\,(K_{max}/K_{Ic}) \quad \text{(Eq 10)}$$

This emphasizes the very important role of compressive residual stresses generated during fatigue precracking in delaying the initiation of SCC processes, i.e., the threshold $K_{ISCC}$ ($K_{IHAC}$ or $K_{ILAD}$) is clearly dependent on residual stress distributions produced by the fatigue precracking regime and controlled by the maximum stress-intensity factor $K_{max}$.

### 3.3 Consequences in Stress-Corrosion and/or Hydrogen-Assisted Cracking

This section analyzes the consequences of cyclic residual stresses in the development of SCC. Emphasis is placed on the effect of the maximum fatigue precracking load during the last step of precracking ($K_{max}$) on the ulterior crack propagation behavior of the steel in an aggressive environment. The experimental program consisted of slow strain rate testing of a high-strength prestressing steel in the form of hot-rolled bar in aqueous solution, as described elsewhere (Ref 6).

**Macroscopical Analysis.** Figure 5 shows the experimental results in a plot representing the failure load in the solution (divided by the reference value in air) as a function of the electro-

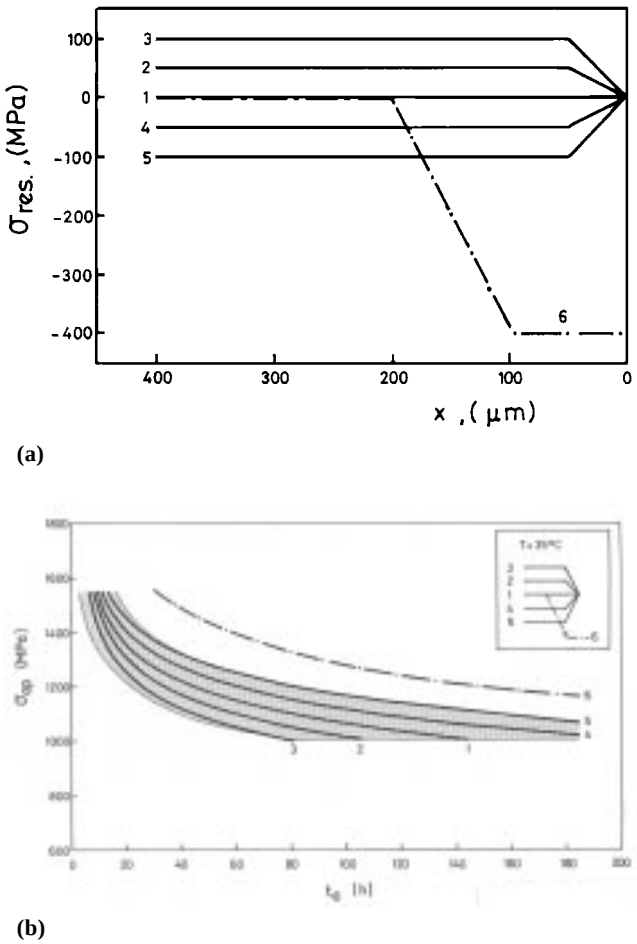


**Fig. 3** (a) Residual stress distributions considered in the computations. (b) Model predictions for the different residual stress laws and comparison with the experimental results of the International Prestressing Federation tests (shaded area)

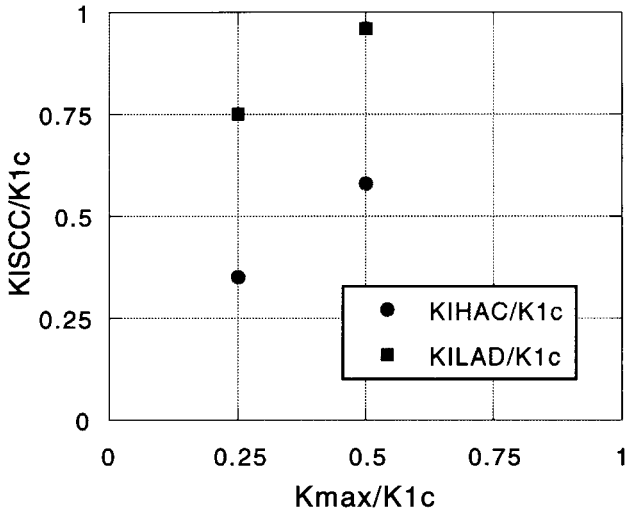


**Fig. 4** Stress-corrosion cracking thresholds $K_{ISCC}$ for hydrogen-assisted cracking ($K_{IHAC}$) and localized anodic dissolution ($K_{ILAD}$) as a function of the maximum stress-intensity factor during the last stage of fatigue precracking ($K_{max}$)

chemical potential. The different curves correspond to diverse overload levels ($K_{max}$).

There are two regions of potential in which the effect of the environment reduces the fracture load: the bottom region is that of the cathodic regime, and the environmental mechanism is hydrogen-assisted cracking, whereas the upper one represents the anodic regime, and the mechanism is localized anodic dissolution.

For both hydrogen-assisted cracking and localized anodic dissolution, the susceptibility to the environment decreases—i.e., the fracture load increases—as the overload increases, and this happens for all values of $K_{max}$. These retardation effects are produced by the presence of compressive residual stresses in the vicinity of the crack tip as a consequence of the cyclic plastic zone created by the fatigue precracking procedure (cyclic residual stresses). In this case the crack tip is, in a certain sense, prestressed by fatigue. The higher the overload level, the more pronounced the prestressing effect, which delays the environmental damage process and improves the material performance in a corrosive environment.

**Microscopical Analysis.** A fractographic analysis by scanning electron microscopy (SEM) was carried out on the fracture surfaces of the samples to detect any effect of residual stresses on the microscopical damage/fracture behavior. Figure 6 shows SEM micrographs for the cathodic regime (hydrogen-assisted cracking, $E = -1200$ mV SCE). Three different microscopic fracture modes can be distinguished in all the micrographs. The left part is the fatigue precracking mode (F), whereas the right one corresponds to the cleavage-like unstable crack propagation (C). Between these two parts a transition topography appears, with microdamage features and different extension depending on the overload $K_{max}$. It is the so-called tearing topography surface (TTS) associated with the hydrogen embrittlement processes in this kind of steel. Figure 6 clearly shows that the TTS size (depth measured in the direction perpendicular to the crack border line) decreases as the fatigue load increases, and thus the TTS extension is about 200 μm for $K_{max} = 0.28\ K_{Ic}$, 125 to 150 μm for $K_{max} = 0.45\ K_{Ic}$, and 10 to 15 μm for $K_{max} = 0.80\ K_{Ic}$.

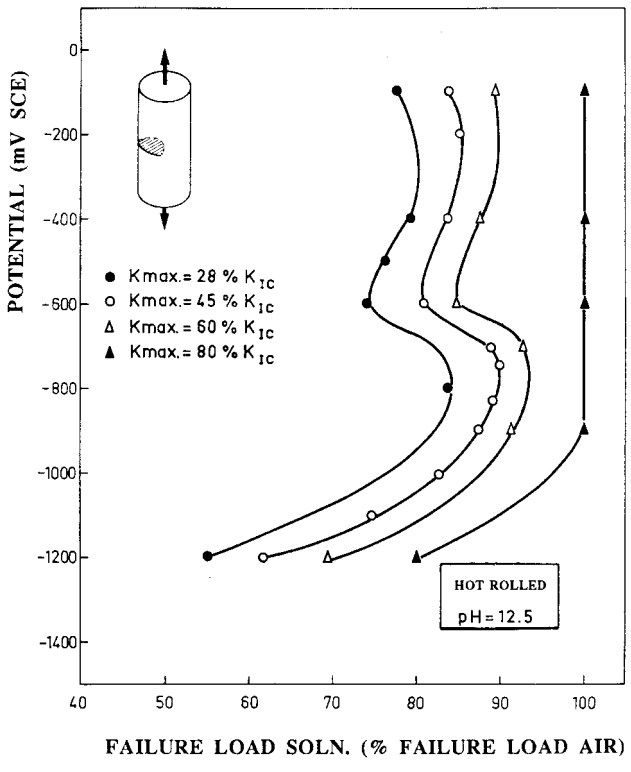


**Fig. 5** Experimental results of slow-strain-rate tests on cylindrical specimens precracked under different $K_{max}$ levels, where $K_{max}$ is the maximum stress-intensity factor during the last step of fatigue precracking

Figure 7 shows SEM micrographs for the anodic regime (localized anodic dissolution, $E = -400$ mV SCE). For $K_{max} = 0.28\ K_{Ic}$, only two microscopic fracture modes can be distinguished, so that a cleavage-like unstable mode of fracture is achieved adjacent to the fatigue precrack. For $K_{max} = 0.80\ K_{Ic}$, a transition topography can be singled out, with a kind of damage appearance. This area is a very narrow band ahead of the crack tip, with an average width of 10 to 15 μm.

**Discussion.** In the case of hydrogen-assisted cracking (Fig. 6), the fact that TTS depth decreases as the fatigue load increases reveals an important effect of the compressive residual stresses generated during fatigue precracking, which delay the hydrogen entry from the solution into the metal, thus decreasing the size of the process zone and increasing the fracture load. The stronger the overload level, the higher the compressive residual stresses, and the lower the penetration of hydrogen into the fracture process zone.

For localized anodic dissolution (Fig. 7), the special microscopic failure mode appears only in the case of very strong fatigue overloads, and again it may be attributed to the presence of a intense compressive residual stress field in the area surrounding the crack tip. There is a double effect in this case: overloads produce a certain kind of microdamage in this area (which could explain the microscopic appearance of such a region), whereas the crack tip is prestressed by the negative residual stresses, which delay metal dissolution up to a certain moment at which the material cleaves and final fracture takes place.

### *3.4 Modeling of Cyclic Residual Stress Laws*

It would be useful to know the cyclic residual stress distribution ahead of the crack tip. There are three kinds of difficulty in solving this problem. First, from the theoretical point of view, it is impossible to know the exact stress distribution in the vicinity of the crack tip after fatigue precracking (and therefore prior to the fracture test), because the stress singularity is relaxed by the plastic zone spread. In addition, the numerical approach to the problem (finite element method, boundary integral equation method) is very complex, due to the stress concentration and to the loading/unloading process. Finally, the residual stress distribution after fatigue precracking is representative only at the beginning of the fracture test, because it changes during it. From these considerations it seems that the formulation of a simple model is sufficient indication of the residual stress distribution ahead of the crack tip.

A classical model of compressive residual stresses in the vicinity of the crack tip is that of Rice (Ref 7). This model is applicable to an elastic, ideally plastic, material under cyclic loading, and it predicts the residual stress distribution in front

of the crack tip at the end of the final fatigue precracking step, and therefore prior to an SCC or hydrogen embrittlement test. During this test the residual stresses in front of the crack tip are redistributed as the external load increases, and the compressions become tensions.

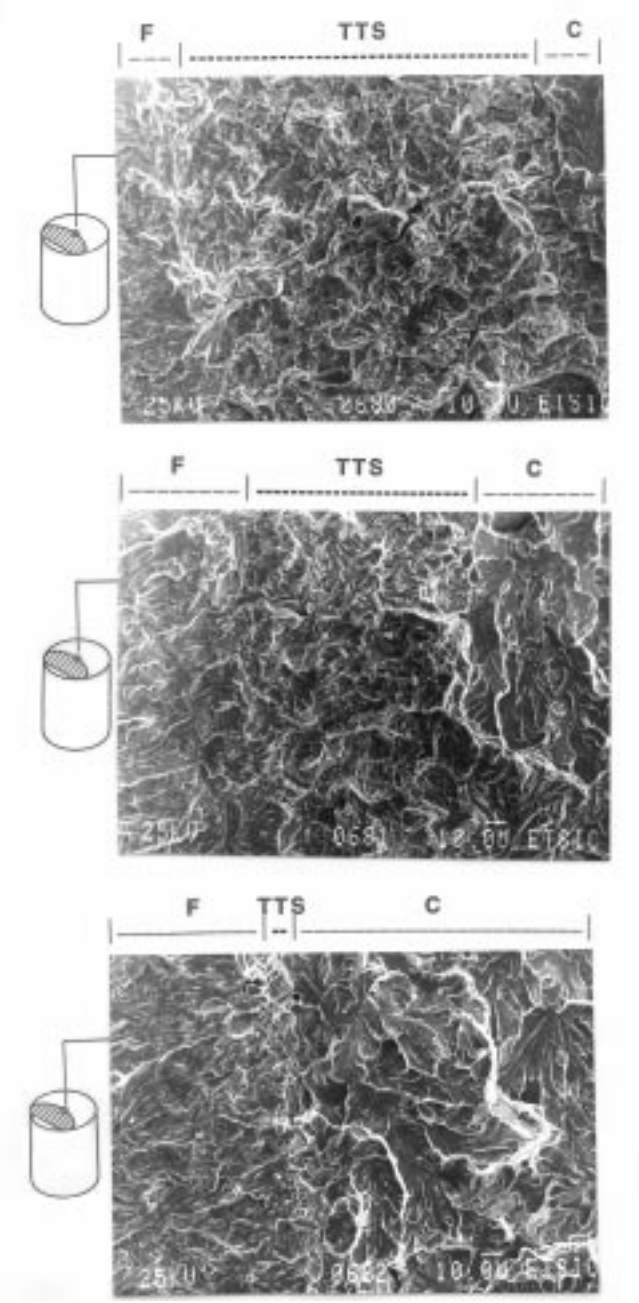


**Fig. 6** SEM micrographs at the crack tip for hydrogen-assisted cracking ($E$ = –1200 mV) and $K_{max}$ = 0.28 $K_{Ic}$ (top), 0.45 $K_{Ic}$ (middle), and 0.80 $K_{Ic}$ (bottom). F, fatigue precrack; TTS, tearing topography surface (transition topography); C, cleavage-like (unstable fracture)

Figure 8 shows the stress distribution proposed by Rice for the maximum ($K = K_{max}$) and minimum ($K = K_{min}$) fatigue loads. In both cases the maximum and minimum stresses are equal to the yield strength of the material $\sigma_Y$ (with positive and negative sign, respectively). Distribution corresponding to $K = K_{min}$ represents the residual stress state after a cyclic loading/unloading process similar to that of fatigue precracking (prior to any stress corrosion test with precracked specimens). As depicted in this plot, cyclic residual stresses ahead of the crack tip are compressions.

The values of ω and Δω represent the depth of the monotonic ($K_{max}$) and cyclic ($K_{min}$) plastic zones respectively, and their values are given by (Ref 7):

$$\omega = \frac{\pi}{8}\left(\frac{K_{max}}{\sigma_Y}\right)^2 \qquad \text{(Eq 11)}$$

$$\Delta\omega = \frac{\pi}{32}\left(\frac{\Delta K}{\sigma_Y}\right)^2 \qquad \text{(Eq 12)}$$

where $\sigma_Y$ is the yield strength of the material, $K_{max}$ is the maximum stress-intensity factor during fatigue precracking (last step of loading, just prior to the SCC test), and $\Delta K$ is the stress-intensity range in that step ($\Delta K = K_{max} - K_{min}$).

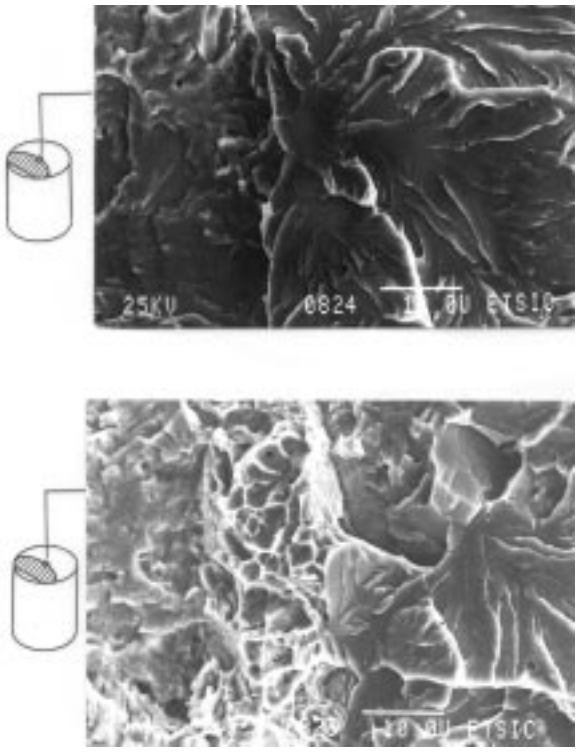


**Fig. 7** SEM micrographs at the crack tip for localized anodic dissolution ($E$ = –400 mV) and $K_{max}$ = 0.28 $K_{Ic}$ (top) and 0.80 $K_{Ic}$ (bottom). For the latter value there is a transition topography between the fatigue precrack and the cleavage-like unstable mode of fracture.

Precracking stress distribution (that of the last peak of tensile load in fatigue) is recovered when the tensile load is applied in the fracture test, i.e., compressive residual stresses are deleted when the specimen is reloaded up to the same tensile stress level as during fatigue. Consequently, for SCC testing with precracked specimens, slow strain rate testing in the cathodic regime (hydrogen-assisted cracking) should be performed at the minimum possible strain rate, to allow enough time for hydrogen to diffuse after recovering the initial tensile stress distribution.

### *3.5 Modeling of the Environmental Process: Hydrogen Diffusion at the Crack Tip*

This section is focused on the modeling of diffusion under dynamic loading with special emphasis on slow-strain-rate testing conditions. A numerical procedure is used to simulate crack-tip hydrogen concentration distributions affected by near-tip elastoplastic stress fields, as described elsewhere (Ref 8).

To model the environmental process, the boundary-value problem of hydrogen diffusion in the vicinity of the crack tip was solved numerically using the DuFort–Frankel scheme. The evolution of hydrostatic residual stresses was modeled as depicted in Fig. 9(a) on the basis of previous computational results (Ref 9). The evolution of hydrostatic stress distribution $\sigma(x)$ is given in the vicinity of the crack tip, from the cyclic residual stress distribution ($K = 0$) after fatigue loading (unloaded solid) to the tensile residual stress distribution corresponding to the solid loaded at $K = K_{max}$, including also the distributions of hydrostatic stress for intermediate steps of loading (thin inner curves between the initial and final thicker lines).

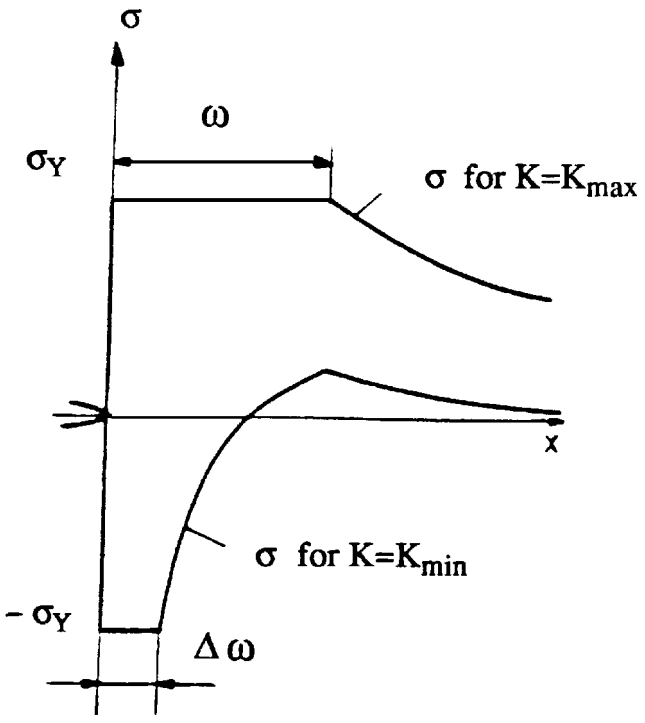


**Fig. 8** Schematic representation of the cyclic residual stress distribution ahead of a crack tip which has (previously) been subjected to far-field cyclic tension, according to Rice's model for an elastic, ideally plastic, material. Source: Ref 7

Figure 9(b) shows the hydrogen concentration profiles for sustained load (solid lines) and rising load associated with slow-strain-rate testing (dashed line) at different times in a dimensionless time scale ($\tau = Dt/x_R^2$). Numerical results demonstrate that hydrogen accumulation in prospective fracture sites near the crack tip during the initial stage of slow-strain-rate testing up to the maximum stress-intensity factor of the crack prehistory displays low sensitivity to loading rate (in terms of stress-intensity factor rate) and strong dependence on cyclic residual stress fields produced at precracking. When near-tip straining proceeds beyond the extent of the residual plasticity influence, the role of loading rate becomes more spectacular. It depends on the diffusion coefficient of hydrogen and on the location of responsible material cells where microfracture proceeds, as well as on the characteristics of material plasticity that define the near-tip stress field at each instantaneous load level.

## 4. Manufacturing-Influenced Cyclic Residual Stresses

### *4.1 Mechanical Effects of Manufacturing a Cold-Drawn Wire*

The effect of cold drawing on the mechanical properties of a (previously) hot-rolled bar is well known and consists of a clear improvement in mechanical properties, which is the main objective of this manufacturing procedure, to achieve a material with a very high yield strength able to undergo intense mechanical levels while at the same time maintaining the elastic range condition.

Apart from manufacturing residual stresses described in a previous section of this paper, cold drawing produces an undesired microstructural effect on the material: a preferential orientation of the pearlite lamellae aligned parallel to the cold drawing direction (Ref 10), resulting in anisotropic properties with regard to fracture behavior in air and aggressive environments. The main consequence is to change the crack propagation direction approaching that of the wire axis (cold drawing direction or main average orientation of the pearlite lamellae) and to produce a mixed-mode state in both fracture in air and in SCC.

The following section describes the consequences of cold drawing on the SCC behavior of cold-drawn wire. It is shown that the improvement of mechanical properties as a result of cold drawing produces secondary effects in the form of better properties against localized anodic dissolution phenomena, but that on the other hand, it produces poor performance in hydrogen-assisted cracking processes (in comparison with the hot-rolled original steel, which is not cold-drawn). The reason is the combination of the two effects analyzed previously, i.e., residual stresses generated by cyclic loading but influenced by the manufacturing process.

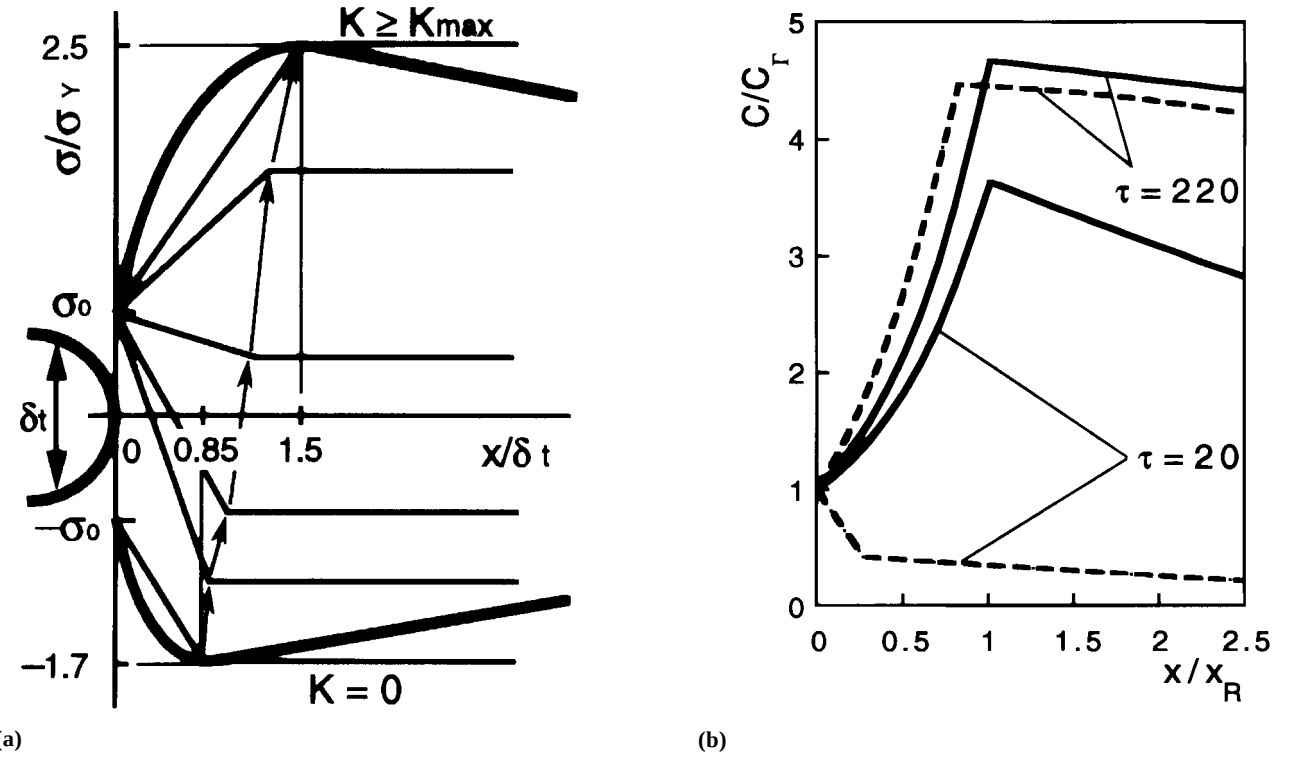


(a) (b)

**Fig. 9** (a) Evolution of hydrostatic stress σ in the vicinity of the crack tip, from $K = 0$ to $K = K_{max}$, where $\sigma_Y$ is the yield strength of the material, $\sigma_0$ is the hydrostatic stress at the crack tip, and $\delta_t$ is the crack tip opening displacement. (b) Hydrogen concentration $C$ at sustained load (solid lines) and slow-strain-rate testing conditions (dashed lines), in a dimensionless time scale $\tau = Dt/x_R^2$, where $C_\Gamma$ is the concentration at the boundary (crack tip), $x_R$ is the depth of the maximum hydrostatic stress point, $D$ is the hydrogen diffusion coefficient, and $t$ is the time. In both figures $x$ is the distance from the crack tip.

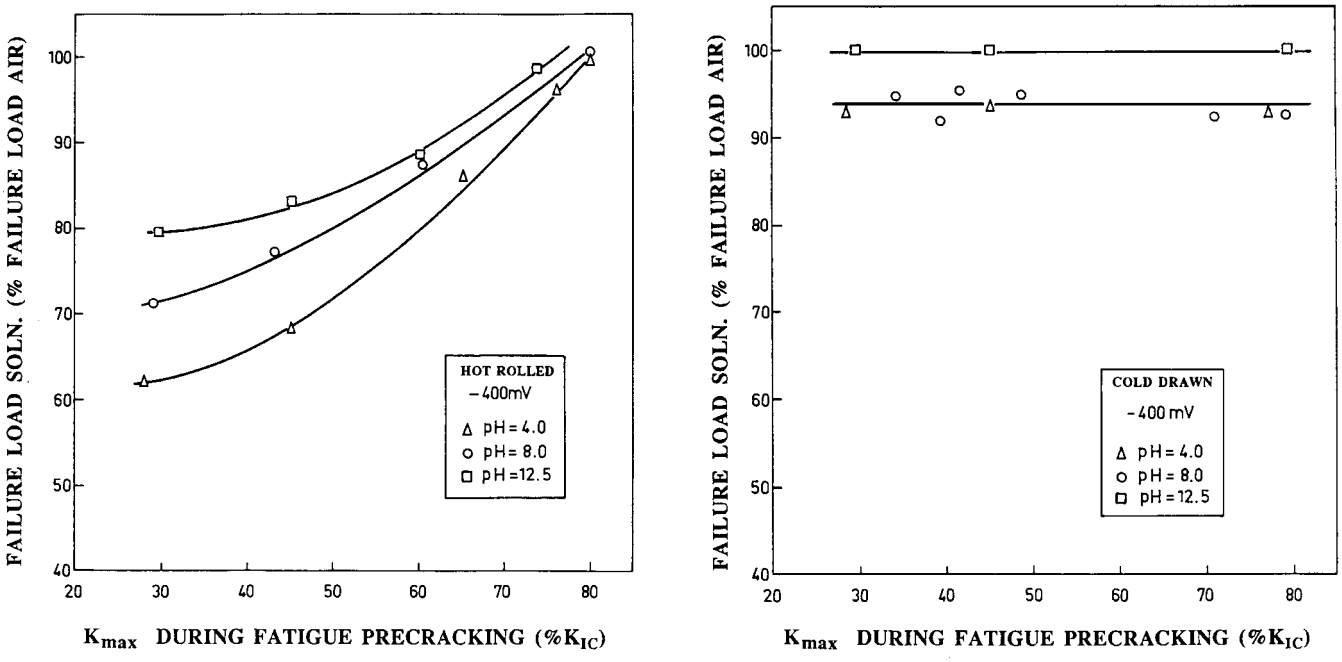


(a) (b)

**Fig. 10** Influence of the fatigue precracking load ($K_{max}$) in the anodic regime (localized anodic dissolution). (a) Hot-rolled bar. (b) Cold-drawn wire

### 4.2 *Consequences in Stress-Corrosion Behavior of the Wires*

This section deals with the consequences of manufacturing-influenced cyclic residual stresses in the stress corrosion behavior of cold-drawn wires (with reference to the hot-rolled bars). The experimental program consisted of slow-strain-rate testing of both hot-rolled bars and cold-drawn wires in aqueous solution, as described elsewhere (Ref 10).

For a typical anodic regime of cracking (–400 mV: localized anodic dissolution), the results depend slightly on pH (Fig. 10). For the hot-rolled bar (Fig. 10a), the test severity decreases as the maximum fatigue load increases. This effect is again due to the compressive residual stresses ahead of the crack tip. The cold-drawn wire (Fig. 10b) is almost insensitive to localized anodic dissolution. The fundamental conclusion is that the cold drawing process is beneficial for the SCC performance at anodic potentials (anodic dissolution or pure SCC).

For a typical cathodic regime (–1200 mV: hydrogen-assisted cracking) the results are practically independent of pH (Fig. 11). For the hot-rolled bar (Fig. 11a), the test severity decreases as the maximum fatigue load increases, and this occurs for all values of $K_{max}$. For the cold-drawn wire (Fig. 11b), the effect is the same from the qualitative point of view (tendency), but not from the quantitative point of view (numerical values), because for all variability ranges of $K_{max}$ the behavior of the cold-drawn steel is clearly below that of the hot-rolled steel. Moreover, there are certain $K_{max}$ values ($K_{max} < 0.50\ K_{Ic}$) for which the effect of the maximum fatigue load on the susceptibility of the cold-drawn wire to hydrogen embrittlement is negligible. The conclusion is that the cold drawing process is damaging for the SCC performance at cathodic potentials (hydrogen-assisted cracking), in spite of the improvement of mechanical properties that it imparts to the steel. Therefore, the advantage of high strength, and subsequently increased bearing capacity in air environment, is offset by the disadvantage of high susceptibility to hydrogen embrittlement.

### 4.3 *Modeling of the Environmental Process*

This section is devoted to discussing why there is such paradoxical behavior of the two steels in hydrogen environment, with consideration of the important role of cyclic residual stress distribution in the vicinity of the crack tip, which is modeled in a simple way and influences the hydrogen penetration into the sample in both situations (Ref 11). The diffusion model includes not only transport of hydrogen toward the points of minimum concentration, but also toward those regions of maximum triaxial stress state. Diffusion equations are as shown in previous sections of this paper.

The model proposed here allows a first explanation, at least qualitative, of the experimental results for the hydrogen-assisted cracking summarized in Fig. 11. Equations 1 and 2 show the importance, from the hydrogen diffusion point of view, of the hydrostatic stress in the vicinity of the crack tip: hydrogen flows not only toward the places with minimum concentration, but also toward those with maximum tensile hydrostatic stress. As a consequence, compressive residual stresses (created by plasticity in the vicinity of the crack tip during fatigue precracking) reduce hydrogen entry and therefore delay the embrittlement.

Taking into account the mechanical properties of both steels, it can be seen that in the hot-rolled bar (lower yield

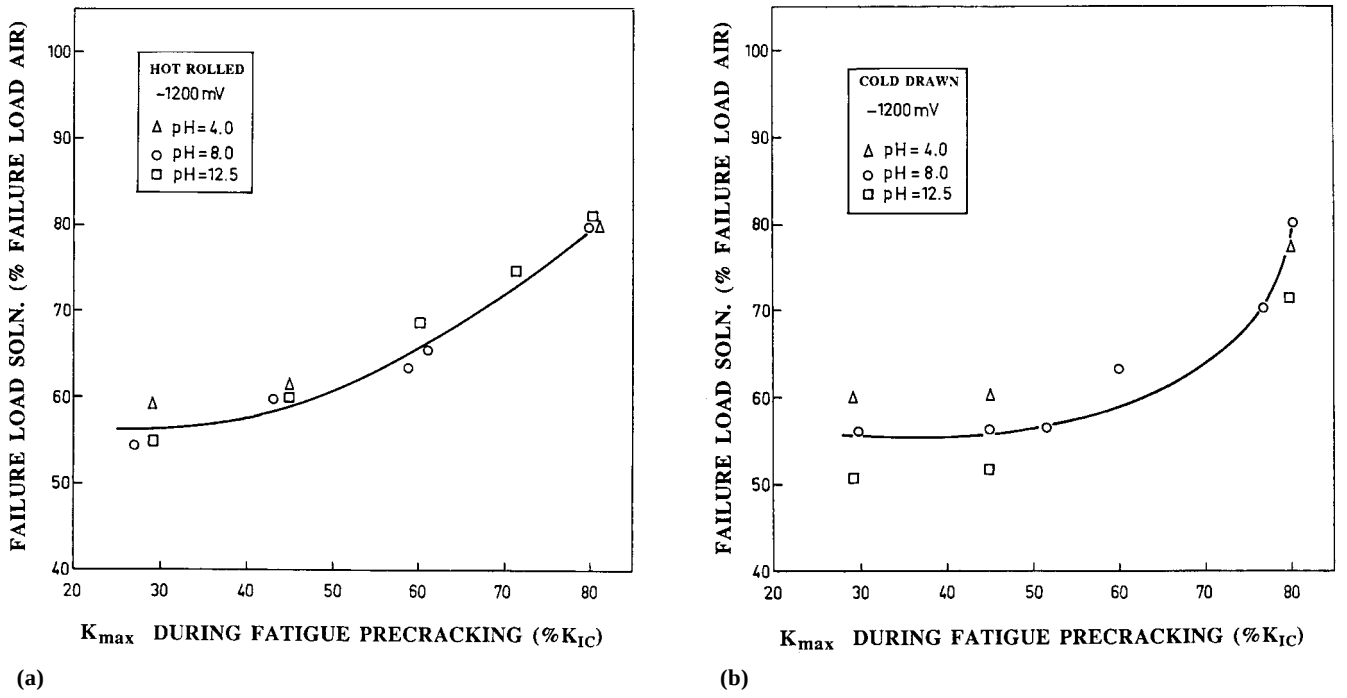


**Fig. 11** Influence of the fatigue precracking load ($K_{max}$) in the cathodic regime (hydrogen-assisted cracking). (a) Hot-rolled bar. (b) Cold-drawn wire

strength) the plastic zone after fatigue precracking is bigger, and the compressive residual stresses in the vicinity of the crack tip are extended along a broader region. This explains the result that the steel of highest yield strength (cold-drawn wire) is the most susceptible to hydrogen embrittlement.

In addition, Rice's model (Ref 7) is able to predict the depth of the maximum hydrostatic stress point, whose importance is determinant in hydrogen diffusion. This point is always at distance w from the crack tip (Fig. 8). For the fatigue precracking tests performed (Ref 11) in all cases $K_{min} \cong 0$, and therefore $\Delta K \approx K_{max}$. Designating $\lambda$ as the dimensionless ratio of the maximum stress-intensity factor during fatigue precracking to the fracture toughness:

$$\lambda = \frac{K_{max}}{K_{Ic}} \quad \text{(Eq 13)}$$

and:

$$\omega = \frac{\pi}{8}\left(\frac{K_{Ic}}{\sigma_Y}\right)^2 \lambda^2 \quad \text{(Eq 14)}$$

$$\Delta\omega = \frac{\pi}{32}\left(\frac{K_{Ic}}{\sigma_Y}\right)^2 \lambda^2 \quad \text{(Eq 15)}$$

where the ratio $(K_{Ic}/\sigma_Y)$ is a characteristic of the material. For the two steels analyzed here, such a distance is $\omega = 2.099\ \lambda^2$ (mm) for the hot-rolled bar and $\omega = 1.232\ \lambda^2$ (mm) for the cold-drawn wire, where $\lambda$ is the dimensionless ratio of $K_{max}$ to $K_{Ic}$ (0.28, 0.45, 0.60, and 0.80). Value $\omega$ is clearly higher for the hot-rolled bar. This length represents the distance that hydrogen has to cover to reach the critical point. Hydrogen concentration at such a point is higher for the cold-drawn wire, because it is nearer the crack tip. As a consequence, the fracture load in hydrogen environment, expressed as a percentage of the fracture load in air, is lower for the cold-drawn steel than for the hot-rolled steel, as depicted in Fig. 11.

These considerations explain why the cold drawing process improves the mechanical properties of the steel while at the same time increasing its susceptibility to hydrogen embrittlement, a problem from this particular point of view.

## 5. Conclusions

- Residual stress fields may be relevant to the SCC performance of structural materials.
- Manufacturing residual stresses may be tensile or compressive, and thus the effect on SCC may be harmful (enhancing the SCC) or beneficial (delaying the SCC).
- Compressive residual stresses generated in cracked elements by cyclic loading have a beneficial (delaying) effect on the SCC performance of the material.
- Manufacturing influences the level of compressive residual stresses produced by cyclic loading in cracked elements and thus affects the SCC behavior.
- The described effects are particularly pronounced in the case of SCC processes in which hydrogen is present (hydrogen-assisted cracking phenomena).


### Acknowledgments

Results summarized in this paper are taken from previous works given in the list of references. Acknowledgment is gratefully given to the co-authors of such papers. In addition, the author wishes to express his gratitude to the Spanish Institutions Comisión Interministerial de Ciencia y Tecnología (CICYT), Dirección General de Investigación Científica y Técnica (DGICYT) and Xunta de Galicia for their financial support to the research under grants MAT91-0113-CE, UE94-001, XUGA 11801A93, and XUGA 11801B95.


### References


1. J.M. Campos and M. Elices, Tensiones Residuales Internas en Alambres Trefilados, *An. Mec. Fract.*, Vol 4, 1987, p 143-157
2. J. Toribio and M. Elices, Influence of Residual Stresses on Hydrogen Embrittlement Susceptibility of Prestressing Steels, *Int. J. Solids Struct.*, Vol 28, 1991, p 791-803
3. J. Toribio, A Computer Model for Predicting the Life of High Strength Steel Wires in $NH_4SCN$ Solution, *Localized Damage II*, Vol 1, *Fatigue and Fracture Mechanics*, M.H. Aliabadi, D.J. Cartwright, and H. Nisitani, Ed., Elsevier, London, 1992, p 581-600
4. "Corrosion of Metals and Alloys—Stress Corrosion Testing," 7539, International Organization for Standardization, 1989
5. J. Toribio and A.M. Lancha, Experimental Evaluation of Environmentally Assisted Cracking: The Effect of Compressive Residual Stresses at the Crack Tip, *J. Mater. Sci. Lett.*, Vol 14, 1995, p 1204-1206
6. J. Toribio and A.M. Lancha, Residual Stress Effects on Stress Corrosion Cracking, *Computer Methods and Experimental Measurements for Surface Treatment Effects II*, M.H. Aliabadi and A. Terranova, Ed., Computational Mechanics Publications, Southampton, 1995, p 163-170
7. J.R. Rice, Mechanics of Crack Tip Deformation and Extension by Fatigue, in STP 415, American Society for Testing and Materials, 1967, p 247-309
8. J. Toribio and V. Kharin, Modeling Hydrogen Diffusion near Crack Tip in Metals: Implications in Slow Strain Rate Testing, *Mechanisms and Mechanics of Damage and Failure—ECF11*, Vol II, J. Petit et al., Ed., EMAS, West Midlands, 1996, p 1569-1574
9. P.C.M. Gortemaker, C. de Pater, and R.M.E.J. Spiering, Near-Crack Tip Finite Strain Analysis, *Advances in Fracture Research—ICF5*, Vol 1, D. Francois, Ed., Pergamon Press, Oxford, 1981, p 151-160
10. J. Toribio and A.M. Lancha, Effect of Cold Drawing on Environmentally Assisted Cracking of Cold-drawn Steel, *J. Mater. Sci.*, , Vol 31, 1996, p 6015-6024
11. J. Toribio and A.M. Lancha, Effect of Cold Drawing on Susceptibility to Hydrogen Embrittlement of Prestressing Steel, *Mater. Struct.*, Vol 26, 1993, p 30-37